Geophys. J. Int. (2009) **179,** 763–777 doi: 10.1111/j.1365-246X.2009.04324.x

Erosional control on the dynamics of low-convergence rate continental plateau margins

V. Godard,[1,2] R. Cattin[1,3] and J. Lavé[4]

[1] *Laboratoire de Géologie,* CNRS-UMR8538*, École Normale Supérieure,* 24 *rue Lhomond,* 75005 *Paris, France. E-mail: godard@cerege.fr*
[2] *CEREGE,* CNRS-UMR6635*, Aix-Marseille Université, Europôle Méditerranéen de l'Arbois,* 13290 *Aix-en-Provence, France*
[3] *Géosciences Montpellier,* CNRS-UMR5243*, Université Montpellier* 2, CC 60, *Place E. Bataillon,* 34095 *Montpellier, France*
[4] *CRPG,* CNRS-UPR2300*, Nancy Université,* 15 *rue N.D. des pauvres,* BP20, 54501 *Vandoeuvre-Lès-Nancy, France*

Accepted 2009 July 6. Received 2009 May 15; in original form 2008 July 10

SUMMARY

Over the last decade, thermomechanical models have revealed the control of both tectonics and erosion on the morphology of continental plateaus margins. However, unravelling the specific effects of these two coupled processes has been difficult in practice. Here, to assess the control of erosion, we investigate the dynamics of the eastern and the northern borders of the Tibetan Plateau, which are characterized by a low convergence rate and a steep topographic escarpment adjacent to the Sichuan and Tarim basins, respectively. Thermomechanical modelling of continental lithosphere coupled with fluvial denudation reveals that important crustal deformation with large-scale horizontal displacements can occur, without any convergence, as a response to mass transfer due to gravitational collapse and to erosional unloading. These processes are sensitive to crustal structure, geothermal gradient as well as surface erosion. At a timescale of several million years, our results suggest that this denudation-triggered deformation exerts a primary control on the evolution of those plateau margins by counterbalancing the mass removal due to erosion and stabilizing the topographic escarpment. This finding supports a possible explanation for the morphology of the Longmen Shan, eastern Tibet, in which the paradoxical combination of persistent high-topographic gradients close to the foreland and low convergence rates can be related to the influence of erosion on deformation patterns.

Key words: Geomorphology; Continental tectonics: compressional; Tectonics and landscape evolution; Rheology: crust and lithosphere; Asia.

1 INTRODUCTION

The evolution of continental relief is controlled by a wide set of factors, which includes both internal and external processes, such as tectonic forcing and erosion. Regional variations of those parameters, in terms of geodynamic or climatic contexts, modulate the shapes, the patterns and the evolution of topography, generating the observed variety of landscapes (e.g. Kooi & Beaumont 1996; Tucker & Slingerland 1997; van der Beek & Braun 1998).

The borders of large continental plateaus, such as the Tibetan Plateau, the Altiplano or the Colorado Plateau, are among the most important topographic structures on Earth. They mark the transition between a low elevated foreland and the high elevation low-relief surface of the plateaus.

The stability in space and time of such features is a matter of debate and the respective contributions of tectonic forcing, erosional unloading and gravitational collapse are not clearly delineated (Masek *et al.* 1994). It is suspected that, at the timescale of mountain building, important couplings and feedbacks exist between internal and external processes (e.g. Molnar & England 1990; Raymo & Ruddiman 1992; Beaumont *et al.* 2001). A better understanding of the dynamics of those regions is thus of a particular interest to put significant constraints on the complex interplay between tectonics and erosion in orogenic setting.

The borders of continental plateaus present a wide range of morphologies. High convergence rate margins are generally associated with high-topographic gradients. However, a few plateau borders have intriguing features with high-topographic gradients typically exceeding 5 per cent and no significant shortening across the margin. Active denudation occurs along some of those margins which, in consequence, are key targets to assess the control of surface processes on lithospheric dynamics. First, because the low shortening rates enables us to assess the geodynamic signal that is only due to erosional unloading. Second, because they raise the question of the nature of the mechanisms needed to maintain such topographic escarpments over long periods of time (several million years).

In this study, we focus on two margins of the Tibetan Plateau, which are among the world's most pronounced topographic escarpments: the eastern and the northern borders of the Plateau. They are both characterized by a low convergence rate and a steep topographic escarpment adjacent to the Sichuan Basin and the Tarim

Basin, respectively. The recent 2008 May $M_w \sim 7.9$ Sichuan earthquake, that occurred along the Longmen Shan range in eastern Tibet, highlights the importance of a better understanding of the geodynamics of such regions.

Our goal is to explore the mechanisms associated with the evolution of those plateau borders under the action of erosion and to investigate how they remain steep and stable through time but we do not investigate in this study the processes leading to the initial topographic building. We will first summarize the general structure and dynamics of those two margins, comparing them with the well-studied southern margin of the Plateau, that is, the Himalayan range, which in contrast, is subject to an intense shortening (Bilham *et al.* 1997; Lavé & Avouac 2000). Next, we will present our modelling strategy, and then explore the different parameters affecting the dynamics of low-convergence margins, with a particular emphasis on the influence of the erosional and thermal regimes. Finally, we will test our modelling results with available data across the eastern and northern Tibetan margins and discuss the paradoxical coexistence of high-topographic gradients and low convergence rates observed in those two areas.

2 GENERAL FEATURES OF TIBETAN MARGINS WITH HIGH-TOPOGRAPHIC GRADIENT

The Tibetan Plateau (Fig. 1) consists in a low relief surface with an average elevation of ∼4000 m (Fielding *et al.* 1994), resulting from the ongoing collision between India and Eurasia. Two end-member models are currently proposed to explain its evolution. Either the strain field in Tibet results from interactions among rigid blocks with localization of deformation along major faults (Avouac & Tapponnier 1993; Tapponnier *et al.* 2001; Thatcher 2007) or the deformation is diffuse and distributed, associated with ductile flow in the mantle and/or in the middle or lower crust (Royden *et al.* 1997; Beaumont *et al.* 2001; Shapiro *et al.* 2004; Klemperer 2006; Copley & Mckenzie 2007). These two end-member models have major implications on the dynamics of plateau borders and they imply different mechanisms for the building and support of high-gradient and low-convergence margins. In one case thrust tectonics is the dominant contribution whereas in the other both thrusting activity and topographic inflation are involved.

In order to provide a consistent framework for our study of those mechanisms, we present the main characteristics of our two areas of interest, the eastern and northern margins of the Tibetan Plateau, and compare them with the well-studied Himalayan southern margin, which present a similar topographic gradient but contrasting tectonic and climatic settings.

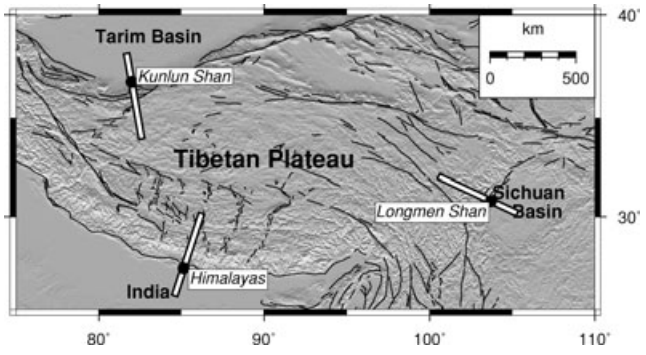

Figure 1. Shaded relief map of the Tibetan Plateau, with the major faults.White lines give the location of the cross-sections presented in Fig. 2.

2.1 Topography and crustal structure

The studied margins are characterized by a sharp topographic transition between the foreland and the Plateau (Fig. 2). For instance, in the Longmen Shan, the topographic transition between the low elevation Sichuan Basin (∼500 m) and the Tibetan Plateau (∼4000 m)

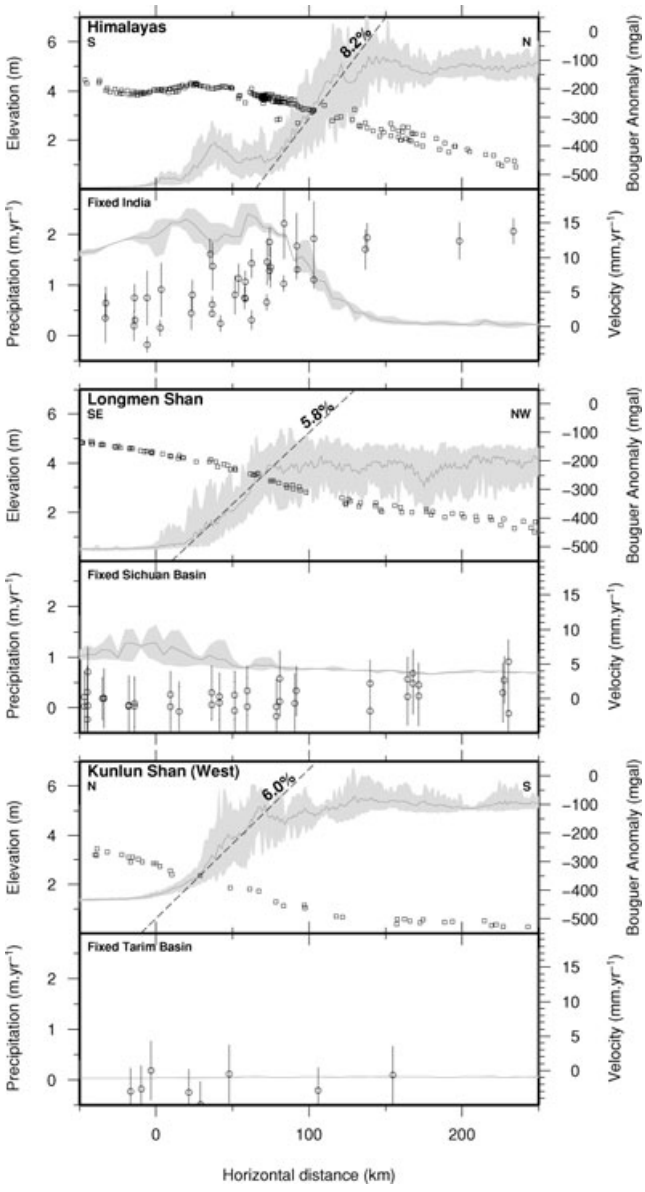

Figure 2. Comparison of topographic, geophysical and precipitation data for Central Nepal (N18 cross-section), Longmen Shan (N295 cross-section) and Kunlun Shan (N170 cross-section), see Fig. 1 for location. Topographic profiles (mean and extreme values) are extracted from ETOPO2 DEM, swathes width is 100 km. Gravity anomaly data are compiled from Sun (1989) and Cattin *et al.* (2001), swathes width is 200 km. Precipitation profiles (mean and extreme values) are extracted from the database of New *et al.* (2002), swathes width is 200 km GPS data are compiled from the works of King *et al.* (1997), Jouanne *et al.* (1999), Larson *et al.* (1999), Chen *et al.* (2000), Zhang *et al.* (2004), Bettinelli *et al.* (2006) and Gan *et al.* (2007), swathes width is 200 km.

is accommodated in ∼60 km of horizontal distance. This leads to a regional topographic gradient of 5.8 per cent, and 6.0 per cent for the Longmen Shan and Kunlun Shan, respectively, which is similar to the 8.2 per cent gradient of the Himalayas. These margins display significant fluvial dissection, contrasting with their flat forelands and the moderate relief of the Plateau.

Moreover, the distribution of Bouguer anomalies, as well as seismic profiles, across those two margins suggest an increase in crustal thickness from 30 to 40 km below the foreland to 50–70 km below the Plateau (Wittlinger *et al.* 1996; Jiang & Jin 2005), which is consistent with Moho deepening across the Himalayan belt (Lyon-Caen & Molnar 1985; Cattin *et al.* 2001; Hetenyi *et al.* 2007).

2.2 Active tectonics

Dense geodetic networks, earthquakes location, as well as geological studies document the distribution and magnitude of deformation across the two studied borders. Low convergence rate is observed across the Longmen Shan range (Fig. 2). In a fixed Sichuan Basin reference frame, GPS velocities are typically <3 mm yr^{-1}, within the confidence range of the measurements (King *et al.* 1997; Chen *et al.* 2000; Shen *et al.* 2005; Gan *et al.* 2007). However, the 2008 May Sichuan earthquake indicates that slow deformation and stress accumulation exist across the Longmen Shan, which is compatible with the low geodetic convergence rates. Lower crustal channel flow propagation is often proposed as a possible mechanism to reconcile the high-topographic gradients of the Longmen Shan margin with this lack of significant surface deformation (Clark & Royden 2000; Clark *et al.* 2005b; Meng *et al.* 2006; Burchfiel *et al.* 2008). In the northern margin, the tectonic setting is different with almost no shortening but significant strike slip motion accommodated along the Kunlun and Altyn Tagh faults (Zhang *et al.* 2004; Gan *et al.* 2007; Jolivet *et al.* 2008). Contrasting with those two low-shortening settings, GPS velocities across the Himalayas give a far-field interseismic convergence rate of 15–20 mm yr^{-1} (Jouanne *et al.* 1999; Larson *et al.* 1999; Bettinelli *et al.* 2006), which is consistent with long-term estimates (Lyon-Caen & Molnar 1985; Armijo *et al.* 1986; Lavé & Avouac 2000).

The three margins are bounded by foreland basins with contrasting histories and sedimentation rates. Late Cenozoic sedimentation is scarce in the Sichuan Basin (Burchfiel *et al.* 1995), which suggests no significant recent flexural loading of this basin by the Longmen Shan. Recent studies suggest that 1–4 km of the sedimentary sequence has been eroded during a mid-Cenozoic exhumation event affecting this basin (Richardson *et al.* 2008). The Tarim Basin area has undergone continuing deformation since the late Precambrian. During the Cenozoic it has developed into a complex system of foreland basins largely in response to the Indo-Asian collision, which led to a Cenozoic sedimentary cover up to 10 km thick in the northern and western part of the basin (Métivier & Gaudemer 1997). Along the Altyn Tagh fault this sedimentary sequence is significantly less developed and flexural loading during the Late Cenozoic was less pronounced than for other borders of the Tarim Basin (Yang & Liu 2002). Similarly, active Cenozoic sedimentation due the flexural loading of the Indian lithosphere by the Himalayan orogen takes place in the Gangetic plain (Hetenyi *et al.* 2006).

2.3 Climate and precipitations

The eastern and northern margins display contrasting climatic contexts (Fig. 2). The eastern margin is influenced by wet tropical climate subjected to monsoon rainfall. Mean annual precipitation can be as high as 1 m yr^{-1} in the Longmen Shan and most of the precipitation occurs during the heavy rains of the summer monsoon. Those climatic conditions in eastern Tibet present similarities with that of the southern margin, even if precipitation is significantly higher in the Himalayas. Also, the Himalayas display a pronounced orographic effect, which leads to a climatic transition from tropical foreland to arid plateau (New *et al.* 2002; Bookhagen & Burbank 2006), with a drop in precipitation from 2 to 4 m yr^{-1} on the Gangetic plain down to 0.2 m yr^{-1} on the Plateau. Such an effect is much more limited across the Longmen Shan due to much lower peak rainfall on the margin and to deep penetration of humid air masses in eastern Tibet during the monsoon (Fig. 2). Both margins have developed extensive ice cover during the glacial periods of the Late Cenozoic, which may have significantly enhanced denudation at high elevations. In contrast, the northern border of the Plateau displays an arid climate with very limited precipitation, mostly because the air coming from the south is depleted of moisture.

3 MODEL DESIGN AND NUMERICAL METHODS

In order to assess the evolution of plateau margins with high-topographic gradients we have developed a 2-D thermomechanical model that incorporates the rheological layering of the continental lithosphere and surface processes. Numerical modelling allows systematic exploration of the implications of variations in the parameters controlling internal and external processes. Such an approach has the potential to deliver insights on the sensitivity of plateau margin dynamics to a range of erosional and rheologic properties.

In previous studies, along with others we have shown that the present-day morphology and dynamics of the Himalayas result from the combination of many factors including shortening rate, fault geometry and erosion processes (Cattin & Avouac 2000; Godard *et al.* 2004, 2006). Due to the significant shortening rate and the complex coupling between tectonics and erosion, the control of erosion on the morphology of the Himalayas is difficult to estimate (Godard *et al.* 2006). Here we focus on the Longmen Shan and Kunlun Shan which are characterized by low shortening rates, in order to assess the specific effects of surface processes acting on those two Plateau borders.

3.1 Physical foundations in the simulations

In this study, we use the CASTEM finite element (FE) package (Verpeaux *et al.* 1988) that we significantly modified to introduce specific solving algorithms for mechanical behaviour integration, rheologies and fluvial incision driven surface processes (Godard 2006).

3.1.1 Mechanical modelling

The solution to the mechanical problem is computed using the FE method, with a time integration based on the dynamic relaxation algorithm (Underwood 1983; Hassani *et al.* 1997). It is applied to the following equation:

$$M\ddot{q} + C\dot{q} + Kq = F_e, \tag{1}$$

with q, $\dot{q}$ and $\ddot{q}$ the displacement, velocity and acceleration vectors, respectively. C is the damping matrix, K the stiffness matrix and F_e the external forces applied on the system. M is the fictitious mass

Table 1. Material parameters used in this study (Carter & Tsenn 1987; Kirby & Kronenberg 1987; Tsenn & Carter 1987; Zhou *et al.* 2000; Wang *et al.* 2000).

	Upper crust	Lower crust	Mantle
Mechanical properties			
Young modulus, E (GPa)	20	20	70
Poisson's ratio, ν	0.25	0.25	0.25
Standard fluidity, γ_0 ($\mathrm{Pa}^{-n}\ \mathrm{s}^{-1}$)	6.03×10^{-24}	6.31×10^{-20}	7.00×10^{-14}
Power law exponent, n	2.72	3.05	3
Activation energy, E_a ($\mathrm{kJ\ mol}^{-1}$)	134	276	510
Density, ρ ($\mathrm{kg\,m}^{-3}$)	2900	2900	3300
Thermal properties			
Conductivity, k ($\mathrm{W\ m}^{-1}\ \mathrm{K}$)	2	2.5	3
Specific heat capacity, C_p ($\mathrm{J\ Kg}^{-1}\ \mathrm{K}$)	1000	1400	1200
Radioactive heat production, H ($\mathrm{W\,m}^{-3}$)	1×10^{-6}	0.4×10^{-6}	2×10^{-9}

matrix. The main advantage of this method is that M can be chosen to be non-singular and easily invertible from a computational point of view. This leads to the following expression that allow the computation of the acceleration field associated with the disequilibrium between external and internal forces,

$$\ddot{q} = M^{-1}\left(-C\dot{q} - Kq + F_e\right). \tag{2}$$

This acceleration field $\ddot{q}$ can be integrated with an explicit finite differences scheme to compute nodal velocities and displacements. In eqs (1) and (2) the quantity $C\dot{q}$ is a numerical viscosity introduced to stabilize the time integration and avoid the development of numerical artefacts. Kq represents the internal forces of the system resulting from the integration of constitutive laws for material behaviour.

The rheology considered in this study is viscoelastic. The elastic part of the behaviour is dictated by Hooke's law (see specification of elastic parameters in Table 1). The non-Newtonian viscous behaviour, dependent on temperature T, is controlled by the following relationship between deviatoric stress and strain rate $\dot{\varepsilon}$:

$$\dot{\varepsilon} = \gamma_0 \left(\sigma_1 - \sigma_3\right)^n \mathrm{e}^{\frac{-E_a}{RT}}, \tag{3}$$

where σ_1 and σ_3 are the maximum and minimum principal stresses, respectively. We calculate the effective Newtonian viscosity ν_{eq} according to

$$\nu_{\mathrm{eq}} = \frac{1}{2\gamma J_2(\sigma')^{n-1}}, \tag{4}$$

where γ is the fluidity of the materials, defined as $\gamma = \gamma_0 \mathrm{e}^{-E_a/RT}$, n is the exponent of the non-linear viscoelastic law (eq. 3) and $J_2(\sigma')$ is the second invariant of the deviatoric stress tensor σ'

$$J_2(\sigma') = \sqrt{3\left(\sigma'^2_{xx} + \sigma'^2_{yy} + \sigma'_{yy}\sigma'_{xx} + \sigma'^2_{xy}\right)}. \tag{5}$$

As detailed below we do not introduce convergence in our models and resulting surface velocities are typically $<0.25\ \mathrm{mm\,yr}^{-1}$. The value of elastic parameters used (Table 1) leads to stress values near the surface that are of the same order of magnitude as the cohesion of rocks ($\sim$10 MPa), and thus limits plastic deformation. Furthermore, comparison of benchmark tests shows that neglecting plastic behaviour has no significant effect on the model outcomes. Thus, in the following we do not use a plasticity criterion.

3.1.2 Thermal modelling

In our modelling, the thermal structure of the crust and mantle is controlled by advection-diffusion heat transport and by heat production due to radiogenic elements. The main factor controlling the evolution of the temperature field is the advection of isotherms due to exhumation in rapidly eroding areas across the plateau border. The heat diffusion-advection equation is solved by the FE method

$$\rho C_p \left(\frac{\partial T}{\partial t} + \vec{u}.\vec{\nabla}\,T\right) = \mathrm{div}\left(k\vec{\nabla}\,T\right) + H, \tag{6}$$

where T is the temperature and $\vec{u}$ the velocity of the material. The values and meanings of the other parameters in eq. (6) are given in Table 1. We impose a constant temperature of 15 °C at the surface and a constant heat flow of 10 $\mathrm{mW\ m}^{-2}$ at the base of the model.

3.1.3 Denudation processes

Fluvial incision related processes play a key role in driving the denudation of continental plateau margins. Those processes are introduced in our simulations through a simple detachment limited fluvial incision law (Howard & Kerby 1983; Lavé & Avouac 2001), where fluvial incision I is proportional to basal shear stress and expressed as

$$I = K A^m S^n, \tag{7}$$

where K is a dimensional erosion efficiency coefficient depending on rock strength, mean precipitation, sediment size and amount and flood distribution. m and n are exponents considered constant, with values of 0.3 and 0.7, respectively (Howard & Kerby 1983; Lavé & Burbank 2004). A is the contributing area, and S is the channel slope. The evolution of A is simply parametrized by imposing the drainage divide at 300 km from the mountain front, so that all water flows towards the foreland, and increasing drainage area linearly to 20 000 km^2 at $x = 0$ km, which is the same order of magnitude as catchments draining those plateau borders. This makes intermodel comparisons easier and is equivalent to imposing a no erosion condition on the Tibetan Plateau. It also prevents the development of instabilities during the initial transient gravitational stabilisation of the model. Slope is directly computed from the geometry of the upper boundary of the model. For Himalayan gneisses and rainfall $\sim$0.7 $\mathrm{m\,yr}^{-1}$, the coefficient K is $\sim$3 $\mathrm{mm}^{0.4}\,\mathrm{yr}^{-1}$ (Lavé & Avouac 2001). Based on this empirical first-order estimate, K will be varied by an order of magnitude around this value, knowing that low (high) precipitation leads to lower (higher) K values.

Following Willett (1999) the fluvial erosion law is directly applied on the model upper boundary rather than on a calculated river profile. In this case, the comparison between topographic data and model outputs is not straightforward because the calculated topography is not equivalent to mean topography or to main trans-range river elevation profile (Lavé 2005; Godard *et al.* 2006). The purpose

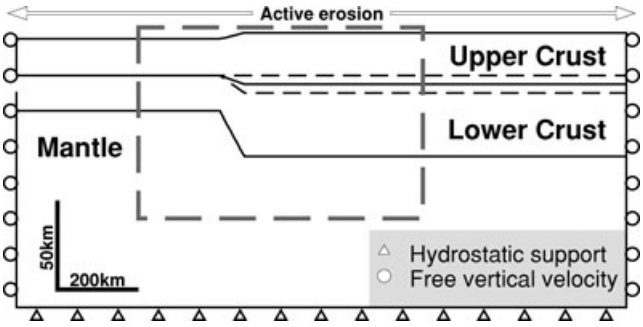

Figure 3. Structure of the mechanical model and boundary conditions used in this study. The black dashed lines indicate different depths for the upper–lower crust boundary tested in this study. The grey dashed box indicates the location of Fig. 5.

of this study is not to propose a best-fitting model for the evolution of either the eastern or northern Tibetan margins, but rather to investigate the general consequences of plateau margin erosion. For that reason we consider that this erosion law captures the main features of denudation processes at the space and timescales we are interested in.

3.2 Geometry and boundary conditions

We use a simplified 2-D geometry (Fig. 3), with isostatically compensated topography that mimics the large wavelengths of both the present-day topography and the crustal structures of eastern and northern borders of the Tibetan Plateau (Fig. 2). We assume a change in elevation of ∼3500 m between the foreland and the Plateau with a topographic gradient of ∼6 per cent. We use a 1500-km-long model to prevent boundary effects (Fig. 3). A temperature and pressure dependent rheology is incorporated for all materials. We assume quartz, diabase and olivine-like rheologies for upper crust, lower crust and mantle, respectively. We use laboratory-derived mechanical and thermal properties for those materials (Table 1) assuming that they can be extrapolated to geological conditions.

The following kinematic conditions on the vertical faces of the model are imposed: vertical displacements are free and horizontal displacements are set to zero. The lithosphere is thus submitted to no convergence. This should be considered as an end-member formulation to simulate the behaviour of low-convergence settings, that allows us to investigate the sole action of erosion over several millions of years. Finally, a hydrostatic foundation is introduced at the base of the model to take into account isostatic support, and simulate the response to erosional unloading.

Slow shortening occurs across those margins (Burchfiel *et al.* 2008; Godard *et al.* in press), but analysing the implications of our simplified definition of the boundary conditions is an important step towards understanding the dynamics of such settings. The purpose of this study is not to propose a best-fitting model for either the Longmen Shan or Kunlun Shan ranges, but rather to test the consequences of a set of simple assumptions concerning the mechanisms involved in the evolution of those plateau margins.

3.3 Numerical stability

3.3.1 Time scenario

Time stepping has a critical importance in controlling the numerical stability when using an explicit solving scheme such as dynamic relaxation. Each numerical experiment simulates 5 Ma of thermo-mechanical evolution with a time step of 1 yr, which is smaller than the relaxation time associated with the lowest viscosity value obtained in our modellings (∼10^{18} Pa s). To avoid sudden perturbations of the system, the erosion of the topographic surface is introduced gradually during the modelling (Fig. 4). The stability of the computation is evaluated using the following inertia ratio criterion

$$I = \frac{||\vec{F}_e + \vec{F}_i||}{||\vec{F}_e|| + ||\vec{F}_i||}, \tag{8}$$

with $\vec{F}_e$ and $\vec{F}_i$ the external and internal forces acting on the system, respectively. I increases with the inertia of the system and tends to zero as the system evolves towards stability.

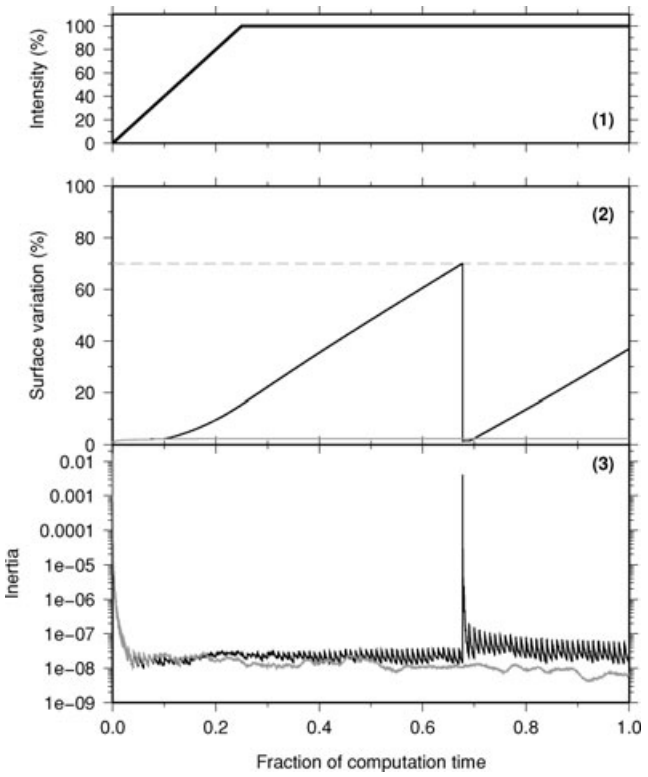

Figure 4. Evolution of the inertia ratio criterion, which defines the stability of the computation. Black and grey plots refer to cases with and without erosion, respectively. (1) Progressive introduction of erosion processes. (2) Deformation of the mesh. The ratio between the surface of the most deformed element with respect to the initial surface is plotted. (3) Evolution of inertia during the computation (eq. 8).

3.3.2 Remeshing

Active denudation induces a decrease in the size of the elements located near the topographic surface. Knowing that the components of the matrix M in eq. (2) are calculated from the ratio between the density and the surface of elements, active erosion is a significant source of instability in a dynamic relaxation based solving scheme. Regular remeshing is thus required to preserve the invertibility of M and the numerical stability of the calculations.

Remeshing is initiated when the surface variation, between the initial and current time step, of the most deformed element of the mesh exceeds a threshold of 70 per cent. All the scalar and vector fields are projected from the old to the new mesh. It is important that

this transfer of information is achieved with minimum discrepancy in equilibrium and constitutive relations. Here, the new values for the fields are estimated from minimization of the following integration for each element of the new mesh:

$$\Delta U = \int_e (U_s - U_e)^2 \, \mathrm{d}s, \tag{9}$$

where U_s and U_e are the final and initial fields values, respectively.

The evolution of both the remeshing and inertia ratio criteria, during a standard simulation, are presented in Fig. 4. The remeshing step is associated with a sudden increase in the inertia of the system. It is a transient perturbation of the mechanical stability of the system. The inertia returns to pre-remeshing values in a time that is short compared to the simulation duration. For a time period of 5 Ma, which typically requires only one remeshing step, our tests show that the remeshing has no significant effects on the results.

4 RESULTS

Here, we present the results relative to the evolution of our thermomechanical models, based on the geometry described in Fig. 3, with rheological parameters set to the values given in Table 1. In a first time we use a fixed erosion efficiency K of 0.4 $\mathrm{mm}^{0.4}\,\mathrm{yr}^{-1}$ in eq. (7), which leads to a maximum erosion rate of $\sim$1 $\mathrm{mm\,yr}^{-1}$ across the plateau margin.

4.1 Crustal deformation

To quantify the control of erosion on plateau-margin dynamics we compare the evolution of two models: one with no erosion and a second one in which the fluvial incision law given in eq. (7) is applied (Fig. 5). Our results illustrate the idea that both gravitational collapse and erosion induce large-scale horizontal crustal displacements below low-convergence margins. Two important shear zones are located at the upper–lower crust transition and at the bottom of the lower crust. The maximum velocity associated with gravitational collapse alone can reach up to 0.2 $\mathrm{mm\,yr}^{-1}$ (Fig. 5a). For the chosen maximum erosion rate of 1 $\mathrm{mm\,yr}^{-1}$, Fig. 5(b) shows that the maximum velocity is $\sim$0.8 $\mathrm{mm\,yr}^{-1}$. This suggests that, for moderate to high erosion rates, the velocity field within the crust of low-convergence margins is primarily driven by active material removal due to erosion across the plateau border. However, if we extrapolate the situation of Fig. 5(b) to low erosion rate ($<$0.3 $\mathrm{mm\,yr}^{-1}$) the contribution of pure gravitational collapse will be dominant. The influence of erosion on crustal velocities decreases with the distance from the plateau margin (x = 0–50 km), and beyond 400 km it is $<$0.2 $\mathrm{mm\,yr}^{-1}$ (Fig. 5b). The normalized velocity field in Fig. 5(c) indicates that the intensity of horizontal velocity between 0 and 200 km, due to the sole influence of active mass removal across the margin, is $\sim$50 per cent of the maximum erosion intensity across the margin. Finally, Fig. 5(d) shows that a two-fold difference in velocity between the two models is still present at 400 km of horizontal distance, and that erosion influences crustal deformation beyond 500 km from the deformation front.

Vertical transects inside the crust for the two studied cases, with and without erosion, are presented in Fig. 6. The velocity profiles confirm the influence of erosion on crustal deformation and the progressive decrease of velocity towards the plateau. Furthermore, the variation of velocity with depth suggests that the displacement of material affects most of the thickness of the crust and that the high velocity zone is shallower near the topographic front. This crustal scale velocity pattern shows a combination of Poiseuille and Couette flows, with a slight displacement of the upper boundary of the deformation zone ($\sim$0.25 $\mathrm{mm\,yr}^{-1}$).

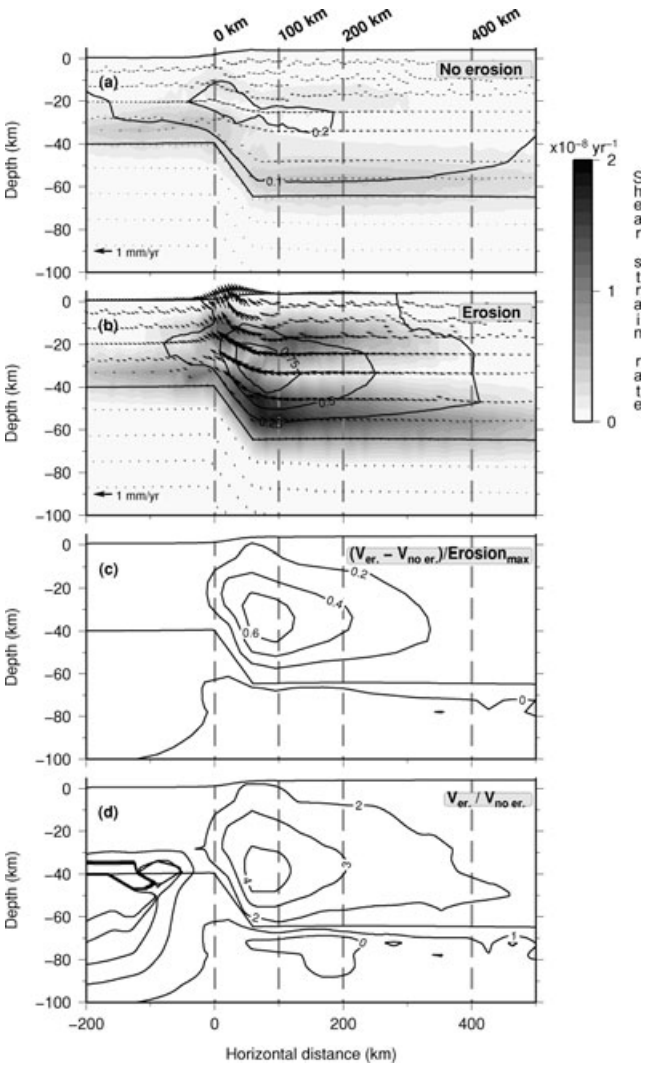

Figure 5. (a) Crustal cross-section showing shear strain rate (gray scale), horizontal velocity values (black contour, in $\mathrm{mm\,yr}^{-1}$) and velocity vectors (black arrows) for modelling without erosion. (b) Same as (a) with erosion. (c) Difference in velocity between the two models, normalized by the maximum erosion rate acting on the margin. (d) Ratio of velocities for the modellings with and without erosion. See Fig. 3 for location. Time is 5 Ma after the beginning of the simulation. Dashed vertical lines indicate the location of the transects presented in Fig. 6.

The calculated geothermal gradients indicate that the thermal state of the crust below the plateau is not significantly affected by the deformation processes occurring at the topographic front (Fig. 6). The slight difference between the two geotherms below the margin (x = 0 km) is associated with the advection of isotherms due to focused erosion in that area. This contributes to a weakening of the upper crust below the topographic front, and such modification can trigger a positive feedback by enhancing further deformation and exhumation. However, in this model, the intensity of denudation is probably not enough to induce a sufficient deflection of the isotherms leading to tectonic aneurysm as proposed by Koons *et al.* (2002) for the Himalayan syntaxes. It can also be noted that the geotherm is slightly hotter than the wet granite solidus at the bottom of the upper crust and that limited partial melting

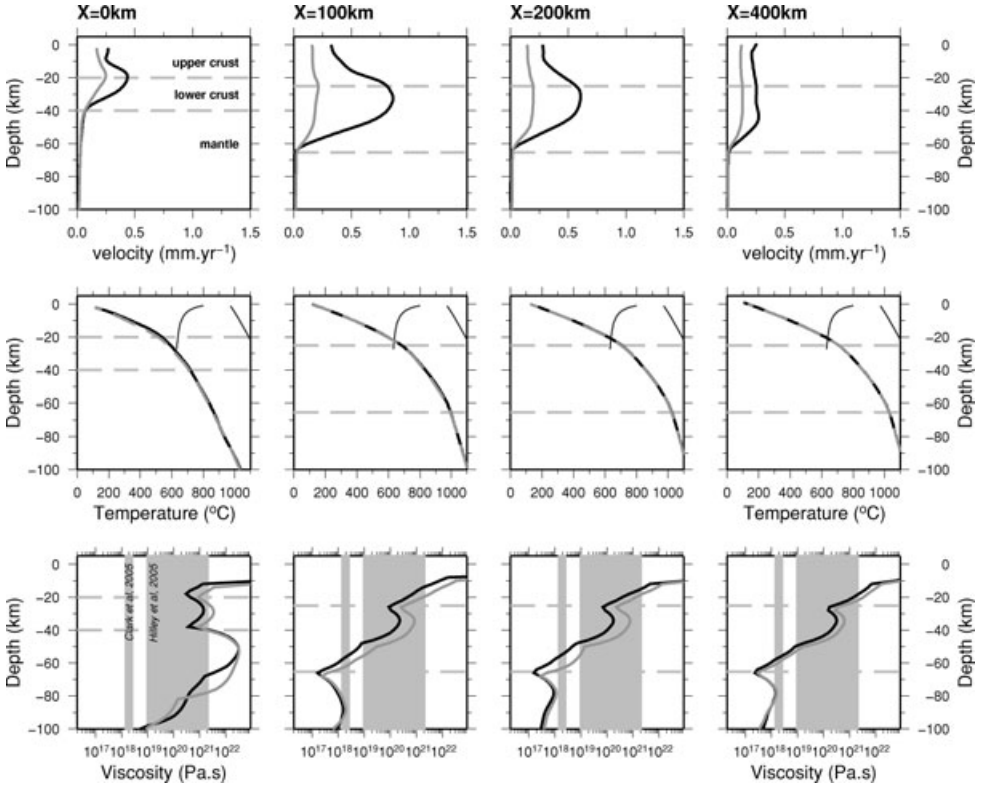

Figure 6. Vertical transects showing the distribution with depth of horizontal velocity, temperature and viscosity. The locations of the transects are indicated in Fig. 5. Black and grey curves represent cases with and without erosion, respectively. Vertical grey boxes indicate crustal viscosities proposed by earlier studies (Clark *et al.* 2005a; Hilley *et al.* 2005b). Horizontal dashed lines indicate the positions of the transition between upper and lower crust and the Moho. In the temperature panels, the dark grey curves in the upper crust represent the wet and dry granite solidii (Holland & Powell 2001).

could occur in that area. Nevertheless, this would require an important hydration of the corresponding materials, which is still largely unconstrained.

The viscosity is temperature dependent and thus rapidly decreases with depth. Within the high-velocity area, the calculated viscosities range from 10^{19} to 10^{21} Pa s, which is consistent with the estimate of Hilley *et al.* (2005a) in northern Tibet and slightly higher than the viscosity proposed for a 15-km-thick channel in the lower crust of eastern Tibet by Clark & Royden (2000) and Clark *et al.* (2005a). Furthermore, our results do not suggest any obvious correlations between the velocity and viscosity profiles. In particular, the depth of the maximum velocity is not related to a local minimum for viscosity.

4.2 Influence of crustal structure

The rheological layering of the continental crust is still poorly constrained, in particular in regions presenting complex tectonic histories such as plateau margins. To assess the sensitivity of our model to variations in the rheological layering, we modify the depth of the upper–lower crust boundary by ± 5 km (Fig. 3) with respect to the previous model (reference model hereinafter). An increase of the thickness of the upper crust leads to a crustal viscosity decrease (Fig. 7), which is a joint effect of both the evolution of the geotherm and the contrasting rheological properties of the upper and lower crusts. Variations of the volume of the radiogenic upper crust affect the thermal structure of the lithosphere, with hotter geotherms associated with a thicker upper crust and the quartz-like rheology implies a relatively soft upper crust, while a diabase rheology results in a stronger lower crust with higher viscosities (Table 1). The viscosity profiles are almost identical in the upper crust, excepted below the lower–upper crust boundary. As the range of variation for the different geotherms is also wider in the lower crust, it can be interpreted as a consequence of the thermal activation of the viscous rheology (eq. 3). In the hotter case associated with the deeper upper–lower crust boundary one can note that the viscosity profile within the crust is consistent with the viscosity proposed by Clark *et al.* (2005a).

Thus, our results confirm that the crustal velocity field is strongly influenced by crustal structure, as the amplitude of velocities is clearly positively correlated with the volume of the upper crust. However, the depth of the maximum velocity does not show any obvious dependency with the depth of the upper–lower crust boundary.

4.3 Influence of thermal and denudation conditions

As proposed by earlier workers (e.g. Beaumont *et al.* 2004) our results suggest an interplay between the intensity of erosion and the thermal state inside the crust, for promoting or inhibiting deformation, and that denudation across the topographic margin triggers large-scale horizontal displacements (Fig. 5). Here we perform a set of simulations where those two processes are varied independently through a simple parametrization in which the thermal regime and the erosion rate are controlled by the radioactive heat production in the upper crust H_{uc} and the coefficient K of eq. (7) (Fig. 8).

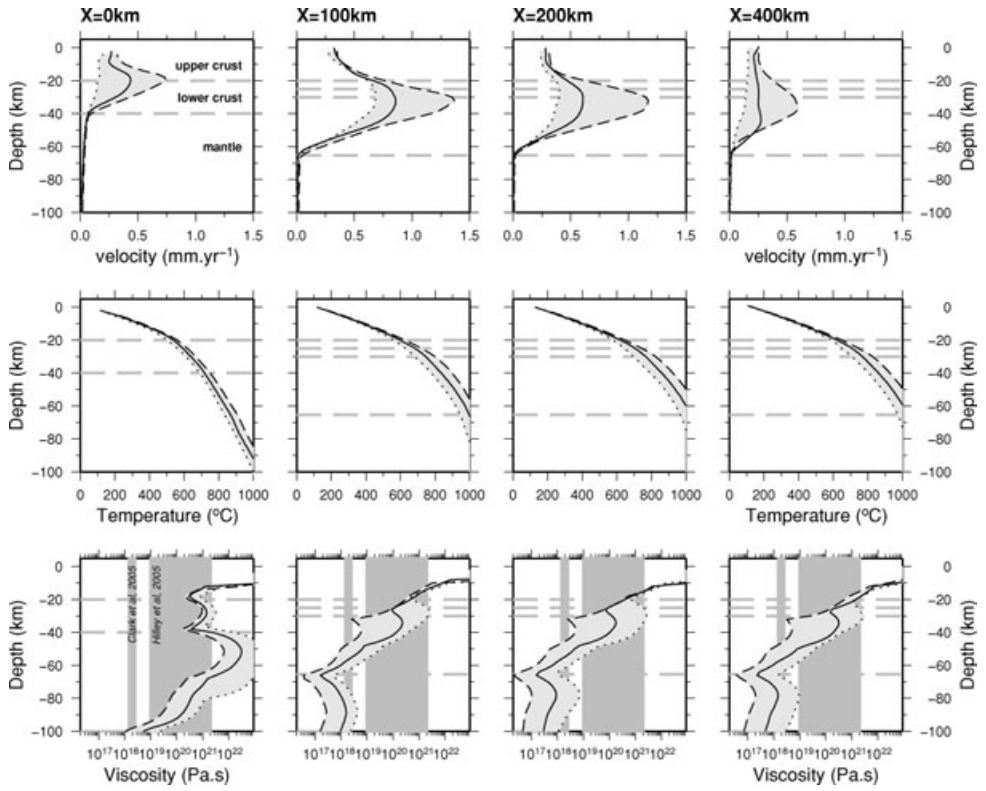

Figure 7. Same as Fig. 6. Black solid curves represent the reference model, with erosion, of Fig. 6. The dashed and dotted black curves represent the cases where the limit between the upper and lower crusts is shifted 5 km downward and upward, respectively (Fig. 3). The horizontal dashed lines indicate the positions of that limit (3 depths tested, Fig. 3) and the Moho.

Our results suggest that the behaviour of the system is sensitive to both parameters (Fig. 8). Low radioactive heat production values ($H_{uc} < 5 \times 10^{-7}$ W m^{-3}) or low erosion values ($K < 0.2$ mm$^{0.4}$ yr^{-1}) preclude the development of significant crustal displacements. Thus, the spread of the orogen is more limited than in the results of Avouac & Burov (1996), which can be related to the specific rigidity of the foreland in our models that prevents the development of such effect.

For the denudation conditions associated with the reference model ($K = 0.4$ mm$^{0.4}$ yr^{-1}), crustal velocity is not steadily increasing with heat production, but reaches a plateau for $H_{uc} > 10^{-6}$ W m^{-3} (Fig. 8b). For high K values erosion is too fast and the crustal flow cannot deliver enough material to compensate what is removed by erosion at the margin. It leads to a propagation of erosion towards the plateau and regressive erosion of the margin.

These results, and the trend of the iso-velocity contours for $K < 0.4$ mm$^{0.4}$ yr^{-1} suggest that erosion is the key parameter in controlling the deformation of the margin and that a hot crust favours the initiation of such deformation. Mean velocity are significantly higher for $K > 0.5$ mm$^{0.4}$ yr^{-1} and $H_{uc} > 10^{-6}$ W m^{-3}, which we interpret as resulting from the initiation of instabilities and major collapse of the margin for vigorous erosion and thermal conditions (Figs 8a and c).

The flow pattern observed in Fig. 5 is the sum of two contributions. First, the gravitational collapse of the margin induces a lateral migration of material and the rigid ramp of the Moho forces this material upward. Second, the denudation across the margin drives exhumation and rock uplift in the upper part of the crust. Interactions and feedbacks exist between those two flow components, but the latter contribution is chiefly modulated by erosion efficiency, whereas the former depends mostly on the plateau gravitational potential energy and the crustal thermal structure, which in turn is controlled by the thermal properties and the intensity of exhumation. The relative positions of the Moho ramp, between the foreland and the plateau, and the topographic margin where erosion is focused, is a critically important factor for the development of crustal movements. In our model, the ramp of the Moho, between the plateau and the basin, is located below the zone of active erosion and facilitates the upward advection of crustal material as a response to gravitational collapse and mass removal across the margin, as illustrated by the velocity pattern in the lower crust (Fig. 5b).

For specific erosion and thermal conditions, local maxima exist for crustal velocities (Fig. 8a). Their existence result from a transition between two regimes for the crustal flow below the margin. In a first case the flow is converging (Figs 5b, 8d and g), with a displacement field advecting material towards the eroding margin, whereas in a second case the flow diverges and exhibits displacement paths in the lower crust not connecting to the surface (Figs 8e and f). This divergence occurs for narrow ranges of erosion rates where the gravitational crustal flow is decoupled from the flow associated with rock uplift across the topographic margin. In this case exhumation is not vigorous enough to divert upward the flow in the middle crust, which is allowed to propagate towards the foreland with high horizontal velocities. The transition between the two regimes is caused by a competition between two distinct effects of erosion: (1) it drives material towards the surface through exhumation and (2) it increases the geothermal gradient, leading to lower viscosity

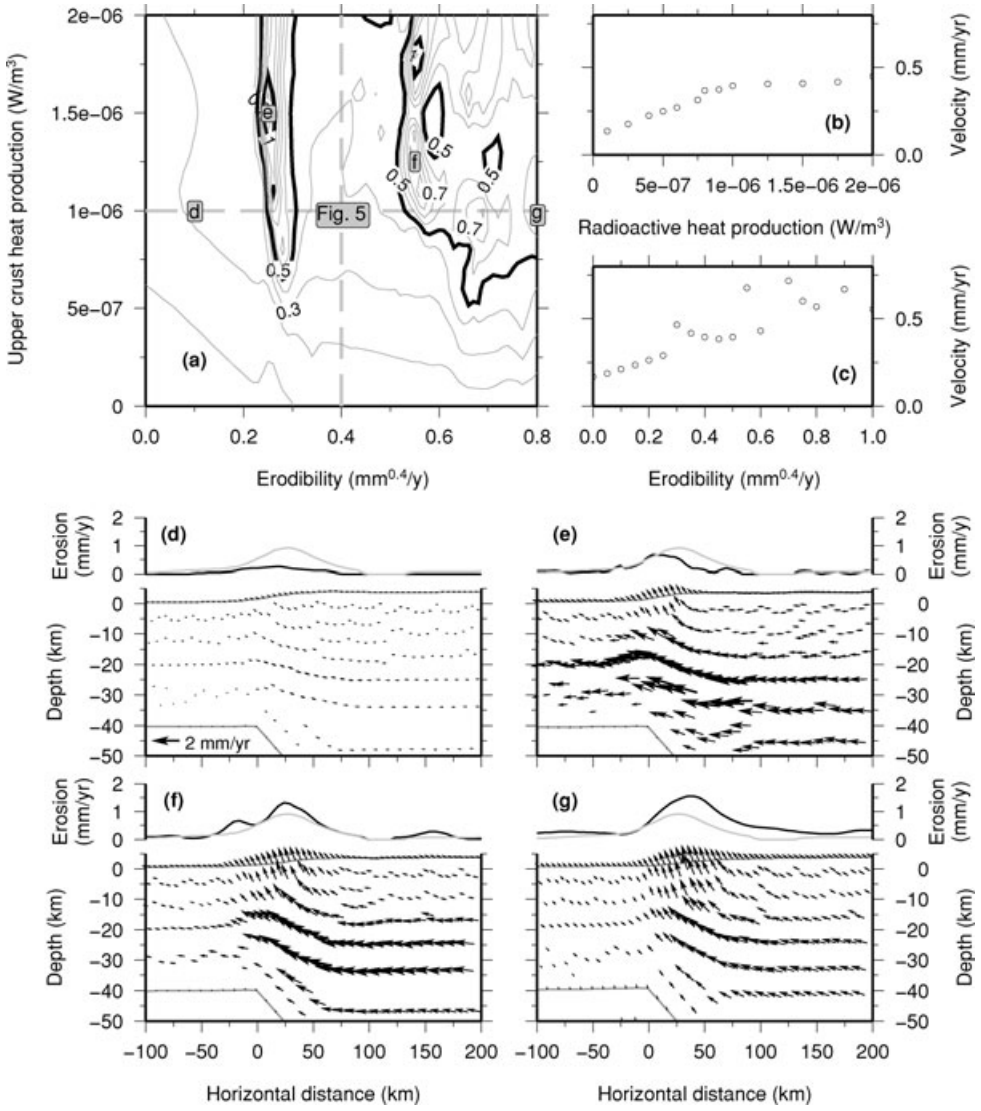

Figure 8. (a) Mean velocity inside the crust beneath the plateau (Fig. 3) for different combinations of erosional and thermal regimes. The grey dashed lines indicate the values associated with the reference model of Fig. 5. (b) Mean velocity for a given erosion efficiency ($K = 0.4$ mm$^{0.4}$ yr^{-1}) and various radioactive heat production values. (c) Mean velocity for a given radioactive heat production ($H_{uc} = 10^{-6}$ W m^{-3}) and various erodibilities values. (d-g) Crustal velocity and erosion profiles for various combination of parameters (see inset a). Grey lines indicate the erosion profile of the reference model of Fig. 5.

(eqs 3 and 4) and an amplification of the ductile gravity-driven flow in the middle crust.

5 APPLICATION TO TIBETAN MARGINS WITH LOW CONVERGENCE AND HIGH-TOPOGRAPHIC GRADIENT

Here we applied our approach to two Tibetan margins (Fig. 9): the Longmen Shan and the Kunlun Shan (see Figs 1 and 2 for location). The gravitational instability associated with the topographic margin induces an important (∼30 km) horizontal collapse just after the beginning of the simulations. To provide a consistent reference frame for comparison with the various data sets, all the model outputs presented in Fig. 9 have been shifted horizontally by the same amount so that the final topography of the model matches the present-day topographic profile. The offsets are 15, 25 and 35 km towards the plateau for the Longmen Shan, Kunlun Shan and no erosion models, respectively.

5.1 Erosion

For both study areas we quantify the intensity of erosion across the margin to adjust the K coefficient of eq. (7). In the Longmen Shan, we compute erosion rates from low-temperature thermochronology data sets (Arne *et al.* 1997; Kirby *et al.* 2002; Godard *et al.* in press), using the geothermal gradient obtained from the computed surface heat flow (Fig. 9c). In the Kunlun Shan denudation over the last 5 Ma is estimated from the sedimentary budgets of Métivier & Gaudemer (1997), that allows to compute a maximum volume for the sediments deposited in the southern Tarim Basin since 5.4 Ma (488×10^3 km^3). Considering the total contributing area for those deposits we obtained a maximum erosion rate <0.5 mm yr^{-1} (Fig. 9g). Indeed, the wet climate of the Longmen Shan promotes active fluvial incision, whereas the dryer northern Tibet presents less pronounced denudation. In the following we assume $K = 0.5$ and 0.2 mm$^{0.4}$ yr^{-1} for the Longmen Shan and the Kunlun Shan, respectively. For both margins uplift and erosion profiles present a similar pattern, with a maximum of erosion and uplift

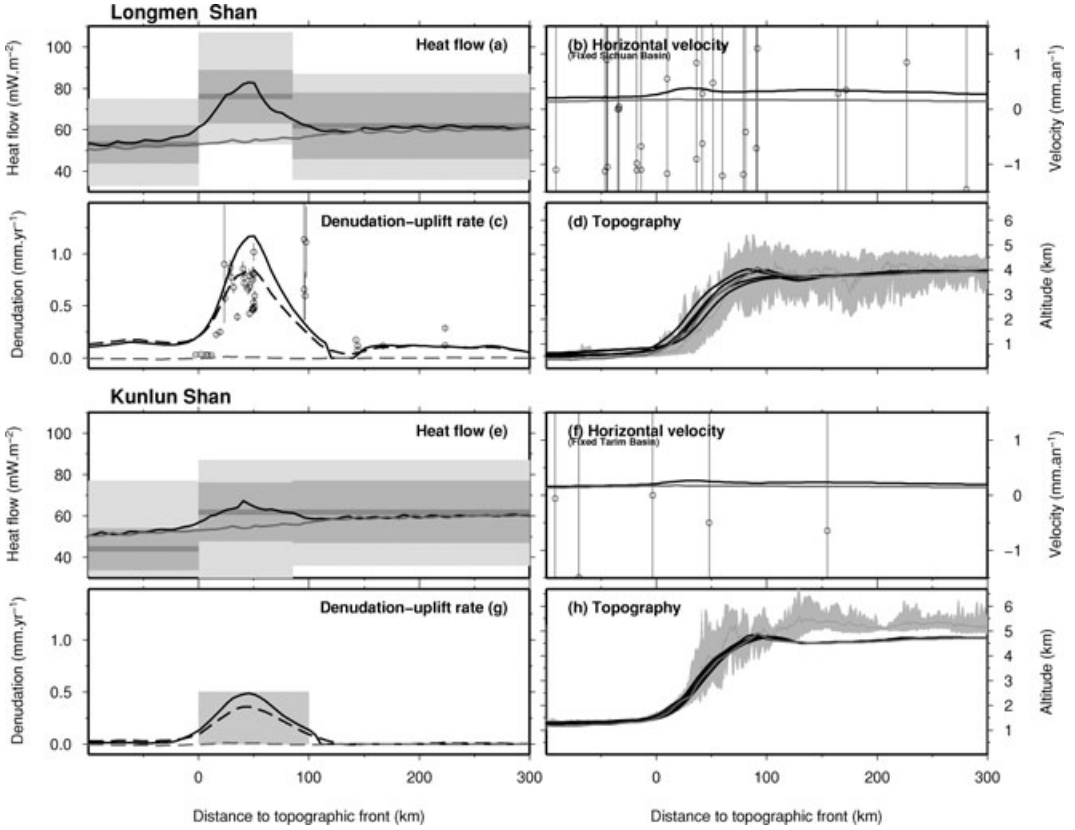

Figure 9. Comparison of modelling outputs (with and without erosion, black and grey curves, respectively) with surface data from the Longmen Shan and Kunlun Shan regions. (a) and (e) Surface heat flow is compared to regional compilations of Hu *et al.* (2000) with, from dark to light grey, mean, $\pm 1\sigma$ and extremal values. (b) and (f) Horizontal velocities confronted to available GPS data (King *et al.* 1997; Chen *et al.* 2000; Zhang *et al.* 2004; Gan *et al.* 2007). (c) and (g) Solid and dashed lines show the calculated erosion and uplift rates, respectively. Erosion rates are derived from various set of thermochronological data in the Longmen Shan (Arne *et al.* 1997; Kirby *et al.* 2002; Godard *et al.* in press) and sediment budget in the Tarim Basin (Métivier & Gaudemer 1997). (d) and (h) Upper boundary of the mechanical model. For the case where erosion is taken into account (black line) several time steps are plotted between the initial state and 5 Ma of simulation. Data sets used for comparison with model outputs are mean and extremal altitudes.

at the Plateau border. This is consistent with the denudation pattern proposed by Kirby *et al.* (2003) in the Longmen Shan.

5.2 Heat flow

The thermal parametrization of the models, and in particular the heat production value in the upper crust, gives calculated heat flows on the Plateau that are consistent with available data ($\sim$50 mW m^{-2}). The data also indicates that both margins are places of high heat flow, in particular the Longmen Shan, with values between 53 and 107 mW m^{-2} (Hu *et al.* 2000; Zhou *et al.* 2000). In both cases the heat flow is significantly higher on the Plateau than in the foreland. Comparison of the eastern and northern Tibet models shows that the intensity of heat flow across the plateau margin is directly correlated with the magnitude of erosion. No local maximum for heat flow is observed across the plateau border for the model without erosion. In contrast, our modelling with erosion mimics the observed spatial pattern of heat flow which presents high heat flow across the margin, corresponding to the vertical advection of isotherms by erosion (Fig. 9).

5.3 Horizontal velocity

Modelling with and without erosion predict low horizontal velocities, that are consistent with available geodetic data (King *et al.* 1997; Chen *et al.* 2000; Zhang *et al.* 2004; Gan *et al.* 2007). Horizontal velocity is slightly influenced by the magnitude of erosion: increased erosion rates lead to increased surface velocities on the Plateau and favour small extension within the margin. This can be related to the modification of the thermal structure due to the upward advection of isotherms, which promotes gravitational collapse towards the foreland.

In the Longmen Shan model, the shortening rate across the topographic margin induced by the Couette flow component of the crustal spreading is $\sim$0.25 mm yr^{-1}. Assuming a dip angle between 30° and 50° for the frontal structure that ruptured during the 2008 May earthquake (USGS 2008), it corresponds to a long-term thrusting slip rate of 0.3–0.4 mm yr^{-1}. This slip rate is lower than the actual long-term slip rate, derived from low temperature thermochronology, that is constrained to between 0.4 and 1 mm yr^{-1} (Godard *et al.* in press). However it suggests that a significant amount of the loading and strain accumulation on the frontal faults of the Longmen Shan can be attributed to gravitational collapse and erosion.

5.4 Topography

We have not distinguished the topography and the upper bound of the mechanical model. This prevents a detailed analysis of the calculated topography. Thus, in the following, we favour a qualitative comparison with the present-day topography.

The topographic evolution of continental passive margin escarpments submitted to active erosion and isostatic support has already been investigated (Gilchrist & Summerfield 1990; Kooi & Beaumont 1994; van der Beek *et al.* 2002). The originality of our approach is to consider a coupling of denudation processes with a thermomechanical model.

For both simulations erosion rates are slightly higher than uplift rates (Figs 9c and g). A significant part of this rock uplift is a consequence of the erosion-driven advection of crustal material towards the surface. It balances the action of erosion and mitigates the retreat of the topographic margin. On the long-term (several millions of years) rock uplift contributes to the stability of the escarpment that remains close to the foreland basin. This phenomenon is illustrated by the different time snapshots of the evolution of the upper boundary of the mechanical model between 0 and 5 Ma that show a preservation of the initial topographic gradient and no large-scale displacement of the margin (Figs 9d and h).

6 DISCUSSION

6.1 Effects of erosion on crustal dynamics

Over the last two decades the influence of erosion on the evolution of active mountain ranges has received particular attention (Beaumont *et al.* 1992; Avouac & Burov 1996; Willett 1999; Beaumont *et al.* 2001, 2004). It has been pointed out that the spatial distribution of mass removal by erosion in actively uplifting settings may critically control the intensity and patterns of tectonic strain. However the relative effects of tectonics and erosion are still debated, partly because of the coupling of these two processes. Here, to overcome this issue, we have developed a modelling approach with no tectonic forcing. A similar approach has already been proposed to investigate the topographic evolution of continental passive margin escarpments (Gilchrist & Summerfield 1990; Kooi & Beaumont 1994; Tucker & Slingerland 1994; van der Beek *et al.* 2002; Braun & van der Beek 2004). However, the results of these studies cannot be applied to Tibetan Plateau borders for the following reasons: (1) their thermal structure is significantly colder, as most of them are developed on old cratonic lithosphere and present significantly lower crustal thicknesses than the Tibetan Plateau, (2) such settings present less important differences in altitude through their escarpments, which implies lower gravitational instabilities and less active regional denudation and (3) those studies are not considering the full thermomechanical behaviour of the lithosphere but only a flexural isostatic response. Therefore, they cannot take into account large-scale horizontal displacements which, as we show in our study, play a major role in the dynamics of the plateau margins.

We show that the evolution of low-convergence margins is sensitive to the intensity of erosion acting across the topographic step. Erosion can induce large-scale deformation inside the crust beneath the plateau (Fig. 5) with velocities of the same order of magnitude as the erosion applied to the margin. A hot crustal geotherm is a necessary condition, but not a sufficient one, to generate such deformation (Fig. 8). Gravitational collapse alone only induces modest crustal velocities. Large magnitude deformation does not occur unless active erosion removes mass across the margin and forces advection of material from the plateau (Fig. 5). With erosion rate high enough to induce crustal deformation, our modellings indicate that the crustal structure and geotherm significantly modulate the velocity amplitude.

The transposition of our results to active mountain range settings suggests that a significant part of the observed deformation could be attributed to the sole interplay between active erosion and large-scale distribution of gravitational potential energy associated with regional topographic gradients. Thus, understanding the exact nature of the interactions between tectonics and erosion in any kind of setting requires evaluating the importance of this contribution to the strain field of the mountain range (Beaumont *et al.* 2004).

6.2 Influence of erosion formalism

In our modelling approach we have paid particular attention to the effects of surface processes considering a full mechanical response to erosion, which allows both isostatic rock uplift and horizontal displacements to contribute to the evolution of topography. However, we have not explored the wide set of formalisms for erosion, and in particular the potential range of variation of exponents m and n in eq. (7) that strongly impact on the behaviour of the erosion law (Whipple & Tucker 1999). We have assumed that the standard detachment limited law we used was capturing the large-scale erosion pattern. This formalism implies a self parallel retreat of the plateau margin, whereas others predict a degradation of the topographic escarpment, in particular for different values of n (Tucker & Whipple 2002). Applying the fluvial incision formalism directly on the mean topography of the model is also an important simplification. More complex formalisms taking into account lateral drainages and hill slope relief (Lavé 2005) will lengthen the typical response time of the model to erosion forcing and slow down the retreat of the margin. Also, using Hack's law to relate drainage area with the distance along the profile, instead of the simple linear relationship used here, would modify the shape of the retreating margin.

In the particular context of narrow post-orogenic ranges Baldwin *et al.* (2003) made an extensive exploration for various fluvial incision formalisms, and showed that the topographic decay timescale was 1–10 Ma for standard detachment-limited conditions, but may be significantly lengthened when introducing further complexities such as critical detachment thresholds or shift to transport limited conditions. They also highlighted the fact that taking into account isostatic support induces a $\sim$6-fold increase in that decay time. Thus, even if the settings we are investigating are different from post-orogenic ranges, we suspect that the decay time of the topography may be at least several millions of years. Actually, in our case, the existence of a large plateau behind the topographic front is an additional important factor that substantially extends the duration of the decay. Independent of the parametrization of our erosion law, our results make us confident that, for the time duration of our simulations (5 Ma) and the range of erosion intensity considered, the topographic gradient of the margin is a relatively stable feature that is not subjected to significant degradation.

Furthermore, in the absence of mechanical coupling and considering our formulation of erosion processes, the action of fluvial incision at $\sim$1 mm yr^{-1} on a $\sim$6 per cent topographic gradient should result in a kinematic wave of incision propagating at $\sim$17 km Ma^{-1} towards the Plateau, in the Longmen Shan case (Lavé & Avouac 2001). Such a regressive wave is not observed in our model due to the influence of large-scale crustal deformation, as we discuss in the next section.

6.3 Processes influencing topographic evolution

In our simulations, most of the erosion across the topographic margin is compensated by rock uplift due to isostatic support and lateral

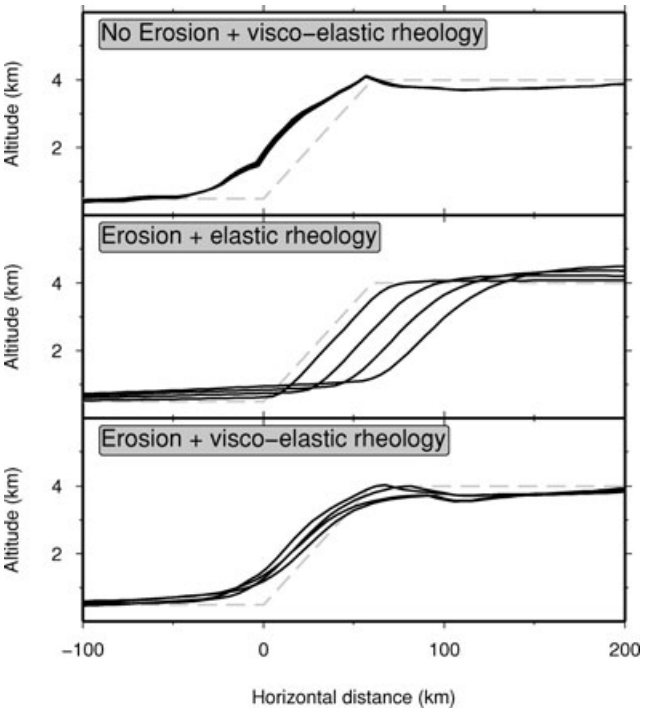

Figure 10. Comparison of topographic margin evolution for different rheologies and erosion conditions. The grey dashed segments indicate the initial topography. The black curves correspond to the same time snapshots as in Fig. 9.

advection of crustal material (Fig. 9). Classical isostatic compensation takes place at the Moho, but in our case the lateral flow allowed by the viscoelastic behaviour compensates a large part of the mass loss due to erosion, which implies that the Moho is significantly deflected upward (Fig. 5b). This denudation-driven flow significantly limits the retreat of the margin and helps to maintain a steep topographic gradient close to the foreland by feeding the crustal exhumation (Fig. 10). The importance of this phenomenon is supported by the retreat of the topographic front over >50 km when considering a simple elastic rheology, whereas the material flow allowed by the viscoelastic behaviour stabilizes the margin and limits the retreat.

An additional factor to preserve topographic gradients across the margin is also the existence of strong structural and rheological contrasts between the plateau and the foreland, as it is the case with the Sichuan and Tarim basins. Indeed, a resistant foreland will limit the gravitational collapse and spreading of the margin. This may explain the singular sharp topography of the eastern and northern borders when compared to other adjacent regions of the Plateau such as southeastern Tibet (Clark & Royden 2000; Clark *et al.* 2005a; Cook & Royden 2008).

6.4 Implications for the eastern Tibetan margin

The coexistence of high-topographic gradients, close to the Sichuan Basin, with modest recent shortening rates across the Longmen Shan is often presented as paradox, that can be explained with the introduction of deep crustal processes such as channel flow in which the topography is dynamically supported by viscous flow within the lower crust (Clark *et al.* 2005a). Based on our numerical modelling (Fig. 10), we interpret this paradox as the result of an interplay between erosion and gravitational collapse which can preserve topographic gradient and curb the retreat of the margin without any internal forcing over several million years (Kirby *et al.* 2002). Several regional studies document a major exhumation event starting between 5 and 15 Ma (Arne *et al.* 1997; Kirby *et al.* 2002; Godard *et al.* in press). This can be associated with an important phase of topographic building in eastern Tibet, and potentially responsible for most of the observed topography across the Longmen Shan. If the main phase of topographic building ceased only a few millions of years ago, the mechanisms that our simulations illustrate could readily explain the persistence of a major escarpment in this area of eastern Tibet, adjacent to the Sichuan Basin, as they tend to mitigate the retreat of the topography. Additionally it has been shown that slow rock uplift is accommodated through the frontal structures of the Longmen Shan (Arne *et al.* 1997; Kirby *et al.* 2002, 2003; Godard *et al.* in press), which has been recently confirmed by the 2008 Sichuan earthquake. This tectonic activity contributes to the preservation of the topographic margin in the Longmen Shan. Even if our end-member modelling does not include discrete fault structures we note that the surface deformation pattern of Figs 5(b), 8(e), (f) and (g) is compatible with this thrusting activity.

The large-scale intracrustal horizontal displacements of material taking place in our experiments share similarities with that proposed by previous studies (Beaumont *et al.* 2004; Clark *et al.* 2005a), but also present distinct features. Notably, as in channel flow models, an important driving force of the flow is the gravitational potential energy and erosion has an important influence in directing the flow and orienting the exhumation paths. However, those displacements are not limited to a narrow channel, but rather they affect a large portion of the Tibetan crust. Likewise, the viscosity profile of Fig. 6 does not present a clear minimum associated with the maximum of the velocity profile. This is an important difference with channel flow models where the existence of very low crustal viscosities is an important requirement to initiate and localize the flow (Beaumont *et al.* 2001; Clark *et al.* 2005a). Our results indicate that standard values for mechanical parameters only allow to reproduce those low viscosities for very hot thermal conditions (Fig. 7). Still, it can be argued that partial melting is likely to occur in the hot and overthickened Tibetan crust. In some of our experiments those conditions may be present at the bottom of the upper crust (Fig. 6), with a small overlap between the geotherm and the wet granite solidus. This partial melting of crustal rocks would likely result in a thin band of weakened material above the limit between the upper and lower crusts, allowing a decoupling between those two compartments.

Finally, in agreement with the channel flow model, our results suggest that the existence of significant structural and rheological contrasts between the plateau and the foreland has an important influence on the orientation of crustal displacements (Clark & Royden 2000; Clark *et al.* 2005a; Cook & Royden 2008). In our case, the ramp of the Moho beneath the topographic margin appears to guide the upward movement of material as a response to focused erosion (Fig. 5).

7 CONCLUSION

Our study is based on an end-member formulation without tectonic shortening, in order to assess the sole influence of erosion acting on plateau margins. Our results reveal that mass removal across plateau borders can trigger important horizontal displacements inside the crust, without internal forcing. Those large-scale deformations

affect the whole crust, over several hundreds kilometres of horizontal distance. The thermal state and structure of the crust can change the nature of the response, but erosion is clearly the main limiting factor to generate those displacements. A direct consequence is that the interplay between erosion and gravitational potential energy can be responsible for a significant part of the global kinematics and strain field in active mountain ranges.

Our study also suggests that high-gradient margins can be stable for several millions of years in those low-convergence settings. This may, in part, reconcile the tectonics and topographic observations in regions such as the Longmen Shan range in eastern Tibet, where the absence of recent shortening and the high-topographic gradients has attracted the attention of researchers over the last decade.

ACKNOWLEDGMENTS

This work was supported by grants from INSU-RELIEF and ANR. All the figures of this article were prepared using the Generic Mapping Tools (GMT) software (Wessel & Smith 1995). Highly constructive and detailed reviews by K. X. Whipple and an anonymous reviewer greatly helped to improve and clarify the article. The manuscript benefited from thorough comments and syntax corrections by J. K. Goode.

REFERENCES

Armijo, R., Tapponnier, P., Mercier, J.L. & Tonglin, H., 1986. Quaternary extension in southern Tibet, *J. geophys. Res.,* **91,** 13 803–13 872.

Arne, D., Worley, B., Wilson, C., Chen, S.F., Foster, D., Luo, Z.L., Liu, S.G. & Dirks, P., 1997. Differential exhumation in response to episodic thrusting along the eastern margin of the Tibetan Plateau, *Tectonophysics,* **280,** 239–256.

Avouac, J.-P. & Burov, E., 1996. Erosion as a driving mechanism of intracontinental growth? *J. geophys. Res.,* **101,** 17 747–17 769.

Avouac, J.P. & Tapponnier, P., 1993. Kinematic model of active deformation in Central-Asia, *Geophys. Res. Lett.,* **20,** 895–898.

Baldwin, J.A., Whipple, K.X. & Tucker, G.E., 2003. Implications of the shear stress river incision model for the timescale of postorogenic decay of topography, *J. geophys. Res.,* **108,** doi:10.1029/2001JB000550.

Beaumont, C., Fullsack, P. & Hamilton, J., 1992. Erosional control of active compressional orogens, in *Thrust Tectonics,* pp. 1–18, Chapman, & Hall, London.

Beaumont, C., Jamieson, R.A., Nguyen, M.H. & Lee, B., 2001. Himalayan tectonics explained by extrusion of a low viscosity crustal channel coupled to focused surface denudation, *Nature,* **414,** 738–742.

Beaumont, C., Jamieson, R.A., Nguyen, M.H. & Medvedev, S., 2004. Crustal channel flows. 1: numerical models with applications to the tectonics of the Himalayan-Tibetan orogen, *J. geophys. Res.,* **109,** doi:10.1029/2003JB002809.

Bettinelli, P., Avouac, J.P., Flouzat, M., Jouanne, F., Bollinger, L., Willis, P. & Chitrakar, G.R., 2006. Plate motion of India and interseismic strain in the Nepal Himalaya from GPS and DORIS measurements, *J. Geod.,* **80,** 567–589.

Bilham, R.K., Larson, K. & Freymuller, J., 1997. GPS measurements of present-day convergence across the Nepal Himalaya, *Nature,* **414,** 61–64.

Bookhagen, B. & Burbank, D.W., 2006. Topography, relief, and TRMM-derived rainfall variations along the Himalaya, *Geophys. Res. Lett.,* **33,** doi:10.1029/2006GL026037.

Braun, J. & van der Beek, P.. 2004. Evolution of passive margin escarpments: what can we learn from low-temperature thermochronology? *J. geophys. Res.,* **109,** doi:10.1029/2004JF000147.

Burchfiel, B. *et al.*, 2008. A geological and geophysical context for the Wenchuan earthquake of 12 May 2008, Sichuan, People's Republic of China, *GSA Today,* **18,** 4–11.

Burchfiel, B.C., Chen, Z., Liu, Y. & Royden, L.H., 1995. Tectonics of the Longmen Shan and adjacent regions, Central China, *Int. Geol. Rev.,* **37,** 661–735.

Carter, N.L. & Tsenn, M.C., 1987. Flow properties of continental lithosphere, *Tectonophysics,* **136,** 27–63.

Cattin, R. & Avouac, J.-P., 2000. Modeling mountain building and the seismic cycle in the Himalaya of Nepal, *J. geophys. Res.,* **105,** 13 389–13 407.

Cattin, R., Martelet, G., Henry, P., Avouac, J.-P., Diament, M. & Shakya, T.R., 2001. Gravity anomalies, crustal structure and thermo-mechanical support of the Himalaya of central Nepal, *Geophys. J. Int.,* **147,** 381–392.

Chen, Z. *et al.*, 2000. Global Positioning System measurements from eastern Tibet and their implications for India/Eurasia intercontinental deformation, *J. geophys. Res.,* **105,** 16 215–16 227.

Clark, M.K. & Royden, L.H., 2000. Topographic ooze: building the eastern margin of Tibet by lower crustal flow, *Geology,* **28,** 703–706.

Clark, M.K., Bush, J.W.M. & Royden, L.H., 2005a. Dynamic topography produced by lower crustal flow against rheological strength heterogeneities bordering the Tibetan Plateau, *Geophys. J. Int.,* **162,** 575–590.

Clark, M.K., House, M.A., Royden, L.H., Whipple, K.X., Burchfiel, B.C., Zhang, X. & Tang, W., 2005b. Late Cenozoic uplift of southeastern Tibet, *Geology,* **33,** 525–528.

Copley, A. & McKenzie, D., 2007. Models of crustal flow in the India-Asia collision zone, *Geophys. J. Int.,* **169,** 683–698.

Cook, K.L. & Royden, L.H., 2008. The role of crustal strength variations in shaping orogenic plateaus, with application to Tibet *J. geophys. Res.,* **113,** doi:10.1029/2007JB005457.

Fielding, E., Isacks, B., Barazangi, M. & Duncan, C., 1994. How flat is Tibet? *Geology,* **22,** 163–167.

Gan, W., Zhang, P., Shen, Z.K., Niu, Z., Wang, M., Wan, Y., Zhou, D. & Cheng, J., 2007. Present-day crustal motion within the Tibetan Plateau inferred from GPS measurements, *J. geophys. Res.,* **112,** doi:10.1029/2005JB004120.

Gilchrist, A.R. & Summerfield, M.A., 1990. Differential denudation and flexural isostasy in formation of rifted-margin upwarps, *Nature,* **346,** 739–742.

Godard, V., 2006. Couplage érosion-tectonique en contexte de convergence intracontinentale. Étude comparée de la chaîne Himalayenne et des Longmen Shan (est-Tibet), *PhD thesis*, Université Paris XI - École Normale Supérieure.

Godard, V., Cattin, R. & Lavé, J., 2004. Numerical modelling of mountain building: interplay between erosion law and crustal rheology, *Geophys. Res. Lett.,* **31,** doi:1.01029/2004GL0210.

Godard, V., J., Lavé, & Cattin, R., 2006. Numerical modelling of erosion processes in the Himalayas of Nepal: effects of spatial variations of rock strength and precipitation, in *Analogue and Numerical Modelling of Crustal-Scale Processes,* Vol. 253, pp. 341–358, eds Buiter, S.J.H. & Schreurs, G., Geological Society, London, Special Publication.

Godard, V., Pik, R., Lavé, J., Tibari, B., Cattin, R., de Sigoyer, J., Pubellier, M. & Zhu, J., Exhumation history of the Central Longmen Shan (Eastern Tibet) from (U-Th)/He thermochronometry, *Tectonics,* in press, doi:10.1029/2008TC002407.

Hassani, R., Jongmans, D. & Chéry, J., 1997. Study of plate deformation and stress in subduction processes using two-dimensional numerical models, *J. geophys. Res.,* **102,** 17 951–17 965.

Hetenyi, G., Cattin, R., Vergne, J. & Nabelek, J., 2006. The effective elastic thickness of the India Plate from receiver function imaging, gravity anomalies and thermomechanical modelling, *Geophys. J. Int.,* **167,** 1106–1118.

Hetenyi, G., Cattin, R., Brunet, F., Bollinger, L., Vergne, J., Nabelek, J. & Diament, M., 2007. Density distribution of the India plate beneath the Tibetan plateau: geophysical and petrological constraints on the kinetics of lower-crustal eclogitization, *Earth planet. Sci. Lett.* **264,** 226–244.

Hilley, G.E., Burgmann, R., Zhang, P.Z. & Molnar, P., 2005a. Bayesian inference of plastosphere viscosities near the Kunlun Fault, northern Tibet, *Geophys. Res. Lett.,* **32,** doi:10.1029/2004GL021658.

Hilley, G.E., Blisniuk, P.M. & Strecker, M.R., 2005b. Mechanics and erosion of basement-cored uplift provinces, *J. geophys. Res.,* **110,** doi:10.1029/2005JB003704.

Holland, T. & Powell, R., 2001. Calculation of phase relations involving haplogranitic melts using an internally consistent thermodynamic dataset, *J. Petrol.,* **42,** 673–683.

Howard, A.D. & Kerby, G., 1983. Channel changes in badlands, *Geol. Soc. Am. Bull.,* **94,** 739–752.

Hu, S.B., He, L.J. & Wang, J.Y., 2000. Heat flow in the continental area of China: a new data set, *Earth planet. Sci. Lett.,* **179,** 407–419.

Jiang, X. & Jin, Y., 2005. Mapping the deep lithospheric structure beneath the eastern margin of the Tibetan Plateau from gravity anomalies, *J. geophys. Res.,* **110,** doi:10.1029/2004JB003394.

Jolivet, R., Cattin, R., Chamot-Rooke, N., Lasserre, C. & Peltzer, G., 2008. Thin-plate modeling of interseismic deformation and asymmetry across the Altyn Tagh fault zone, *Geophys. Res. Lett.,* **35,** doi:10.1029/2007GL031511.

Jouanne, F., Mugnier, J.-L., Pandey, M.R., Gamond, J.-F., Le Fort, P., Serrurier, L., Vigny, C. & Avouac, J.-P., 1999. Oblique convergence in the Himalayas of western Nepal deduced from preliminary results of GPS measurements, *Geophys. Res. Lett.,* **13,** 1933–1936.

King, R.W. *et al.*, 1997. Geodetic measurments of crustal motion in southwest China, *Geology,* **25,** 179–182.

Kirby, E., Reiners, P.W., Krol, M.A., Whipple, K.X., Hodges, K.V., Farley, K.A., Tang, W.Q. & Chen, Z.L., 2002. Late Cenozoic evolution of the eastern margin of the Tibetan Plateau: inferences from Ar-40/Ar-39 and (U-Th)/He thermochronology, *Tectonics,* **21,** doi:10.1029/2000TC001246.

Kirby, E., Whipple, K.X., Tang, W.Q. & Chen, Z.L., 2003. Distribution of active rock uplift along the eastern margin of the Tibetan Plateau: inferences from bedrock channel longitudinal profiles, *J. geophys. Res.,* **108,** doi:10.1029/2001JB000861.

Kirby, S.H. & Kronenberg, A.K., 1987. Rheology of the lithosphere: selected topics, *Rev. Geophys.,* **25,** 1219–1244.

Klemperer, S.L., 2006. Crustal flow in Tibet: geophysical evidence for the physical state of tibetan lithosphere, and inferred patterns of active flow, in *Channel Flow, Ductile Extrusion and Exhumation In Continental Collision Zones,* Vol. 268, pp. 39–70, eds Law, R.D., Searle, M.P. & Godin, L., Geological Society, London, Special Publication.

Kooi, H. & Beaumont, C., 1994. Escarpment evolution on high-elevation rifted margins, insights derived from a surface processes model that combines diffusion, advection, and reaction, *J. geophys. Res.,* **99,** 12 191–12 209.

Kooi, H. & Beaumont, C., 1996. Large-scale geomorphology: classical concepts reconciled and integrated with contemporary ideas via a surface processes model, *J. geophys. Res.,* **101,** 3361–3386.

Koons, P.O., Zeitler, P.K., Chamberlain, C.P., Craw, D. & Meltzer, A.S., 2002. Mechanical links between erosion and metamorphism in Nanga Parbat, Pakistan Himalaya, *Am. J. Sci.,* **302,** 749–773.

Larson, K., Bürgmann, R., Bilham, R. & Freymueller, J., 1999. Kinematics of the India-Eurasia collision zone from GPS measurements, *J. geophys. Res.,* **104,** 1077–1093.

Lavé, J, 2005. Analytic solution of the mean elevation of a watershed dominated by fluvial incision and hillslope landslides, *Geophys. Res. Lett.,* **32,** doi:10.1029/2005GL022482.

Lavé, J. & Avouac, J.-P., 2000. Active folding of fluvial terraces across the Siwaliks hills, Himalaya of central Nepal, *J. geophys. Res.,* **105,** 5735–5770.

Lavé, J. & Avouac, J.-P., 2001. Fluvial incision and tectonic uplift across the Himalayas of central Nepal, *J. geophys. Res.,* **106,** 26 561–26 591.

Lavé, J. & Burbank, D., 2004. Denudation processes and rates in the Transverse ranges, southern California: erosional response of a transitional landscape to external and anthropogenic forcing, *J. geophys. Res.,* **109,** doi:10.1029/2003JF000023.

Lyon-Caen, H. & Molnar, P., 1985. Gravity anomalies, flexure of the indian plate, and the structure, support and evolution of the Himalaya and Ganga basin, *Tectonics,* **4,** 513–538.

Masek, J.G., Isacks, B.L., Gubbels, T.L. & Fielding, E.J., 1994. Erosion and tectonics at the margins of continental plateaus, *J. geophys. Res.,* **99,** 13 941–13 956.

Meng, Q.R., Hu, J.M., Wang, E. & Qu, H.J., 2006. Late Cenozoic denudation by large-magnitude landslides in the eastern edge of Tibetan Plateau, *Earth planet. Sci. Lett.,* **243,** 252–267.

Métivier, F. & Gaudemer, Y., 1997. Mass transfer between eastern Tien Shan and adjacent basins (central Asia): constraints on regional tectonics and topography, *Geophys. J. Int.,* **128,** 1–17.

Molnar, P. & England, P., 1990. Late Cenozoic uplift of mountain ranges and global climate change: chicken or egg? *Nature,* **346,** 29–34.

New, M., Lister, D., Hulme, M. & Makin, I., 2002. A high-resolution data set of surface climate over global land areas, *Clim. Res.,* **21,** 1–25.

Raymo, M.E. & Ruddiman, W.F., 1992. Tectonic forcing of late Cenozoic climate, *Nature,* **359,** 117–122.

Richardson, N.J., Densmore, A.L., Seward, D., Fowler, A., Wipf, A., Ellis, M.A., Yong, L. & Zhang, Y., 2008. Extraordinary denudation in the Sichuan Basin: insights from low-temperature thermochronology adjacent to the eastern margin of the Tibetan Plateau, *J. geophys. Res.,* **113,** doi:10.1029/2006JB004739.

Royden, L.H., Burchfiel, B.C., King, R.W., Wang, E., Chen, Z.L., Shen, F. & Liu, Y.P., 1997. Surface deformation and lower crustal flow in eastern Tibet, *Science,* **276,** 788–790.

Shapiro, N.M., Ritzwoller, M.H., Molnar, P. & Levin, V., 2004. Thinning and flow of Tibetan crust constrained by seismic anisotropy, *Science,* **305,** 233–236.

Shen, Z.K., Lu, J.N., Wang, M. & Burgmann, R., 2005. Contemporary crustal deformation around the southeast borderland of the Tibetan Plateau, *J. geophys. Res.,* **110,** doi:10.1029/2004JB003421.

Sun, W., 1989. Bouguer Gravity Anomaly Map of the People's Republic of China, Tech. rep., Chin. Acad. Geoexplor. Beijing.

Tapponnier, P., Xu, Z.Q., Roger, F., Meyer, B., Arnaud, N., Wittlinger, G. & Yang, J.S., 2001. Oblique stepwise rise and growth of the Tibet plateau, *Science,* **294,** 1671–1677.

Thatcher, W., 2007. Microplate model for the present-day deformation of Tibet, *J. geophys. Res.,* **112,** doi:10.1029/2005JB004244.

Tsenn, M.C. & Carter, N.L., 1987. Upper limits of power law creep of rocks, *Tectonophysics,* **136,** 1–26.

Tucker, G.E. & Slingerland, R., 1994. Erosional dynamics, flexural isostasy, and long-lived escarpments: a numerical modeling study. *J. geophys. Res.,* **99,** 12 229–12 243.

Tucker, G.E. & Slingerland, R., 1997. Drainage basin responses to climate change, *Wat. Res. Res.,* **33,** 2031–2047.

Tucker, G.E. & Whipple, K.X., 2002. Implications of sediment-flux-dependent river incision models for landscape evolution, *J. geophys. Res.,* **107,** doi:10.1029/2000JB000044.

Underwood, P., 1983. *Dynamic Relaxation. Computational Methods for Transient Analysis,* Elsevier, Amsterdam, pp. 245–265.

U.S. Geological Survey, 2008. National Earthquake Information Center. http://earthquake.usgs.gov/eqcenter/eqinthenews/2008/us2008ryan/.

van der Beek, P. & Braun, J., 1998. Numerical modelling of landscape evolution on geological time-scales: a parameter analysis and comparison with the south-eastern highlands of Australia, *Basin Res.,* **10,** 49–68.

van der Beek, P., Summerfield, M.A., Braun, J., Brown, R.W. & Fleming, A., 2002. Modeling postbreakup landscape development and denudational history across the southeast African (Drakensberg Escarpment) margin, *J. geophys. Res.,* **107,** doi:10.1029/2001JB000744.

Verpeaux, P., Charras, T. & Millard, A., 1988. Castem 2000: une approche moderne du calcul des structures, in *Calcul des Structures et Intelligence Artificielle,* pp. 261–271, eds Fouet, J.M., Ladevèze, P. & Ohayon, R., Editions Pluralis, Paris.

Wang, X., Wang, J., Li, Q. & Yu, H., 2000. Deep heat flow and geothermal structure in Sichuan Basin of China, in *Proceedings World Geothermal Congress,* Kyushu-Tohoku, Japan, pp. 1937–1940, International Geothermal Association, Reykjavik.

Wessel, P, & Smith W.H.F., 1995. New version of the Generic Mapping Tools released, *EOS, Trans. Am. geophys. Un.,* **76,** 329.

Whipple, K.X. & Tucker, G.E., 1999. Dynamics of stream-power river incision model: implications for height limits of mountain ranges, landscape response timescales, and research needs, *J. geophys. Res.,* **104,** 17 661–17 674.

Willett, S.D., 1999. Orogeny and orography: the effects of erosion on the structure of mountain belts, *J. geophys. Res.,* **104,** 28 957–28 981.

Wittlinger, G. *et al.*, 1996. Seismic tomography of northern Tibet and Kunlun: evidence for crustal blocks and mantle velocity contrasts, *Earth planet. Sci. Lett.,* **139,** 263–279.

Yang, Y.Q. & Liu, M., 2002. Cenozoic deformation of the Tarim plate and the implications for mountain building in the Tibetan Plateau and the Tian Shan, *Tectonics,* **21,** doi:10.1029/2001TC001300.

Zhang, P.-Z. *et al.*, 2004. Continuous deformation of the Tibetan Plateau from Global Positioning System data, *Geology,* **32,** 809–812.

Zhou, X., Wang, X., Yang, S., Yu, H. & Zeng, Y., 2000. The analysis of geothermal field characteristics in Sichuan Basin of China, in *Proceedings World Geothermal Congress,* Kyushu-Tohoku, Japan, pp. 1937–1940, International Geothermal Association, Reykjavik.